Numerical convergence on adaptive grids for control volume methods

S. K. Khattri
Department of Mathematics, University of Bergen

I. Aavatsmark
Centre for Integrated Petroleum Research, University of Bergen

An adaptive technique for control-volume methods applied to second order elliptic equations in two dimension is presented. The convergence behavior of this method is investigated numerically. For solutions with low Sobolev regularity, the found L^2 convergence order is 2 for the potential and 1 for the flow density. The system of linear equations is better conditioned for the adaptive grids than for uniform grids. The test runs indicate that a pure flux-based refinement criterion is preferable.

Keywords: Control-volume method, adaptive grids, convergence rate

I. INTRODUCTION

This paper discusses adaptive algorithms for control-volume methods applied to second order elliptic equations in two dimensions. The grids consist of coarse and fine rectangular grid cells.

It is well known that discrete approximations to solutions of second order elliptic equations possess poor convergence properties when the solution has low Sobolev regularity [1, 10, 16]. The purpose of the paper is to investigate if the convergence behavior can be improved by the application of adaptive techniques.

Convergence of control-volume methods has been proved for matching quadrilateral grids [2, 12, 17, 19]. In this paper we apply multipoint flux approximations on non-matching grids, and for this method, no proof exists.

Adaptive techniques have been analyzed and applied with the finite element method [4, 5, 8, 13, 18] and with the mixed finite element method [15]. For control-volume methods, refinement along a curve of finite length has been analyzed [11]. For repeated refinements, numerical tests have been performed [3, 7, 9], but these tests do not cover convergence behavior as a function of Sobolev regularity.

Our applications are solution of multiphase flow equations in subsurface flow [14]. These equations contain an elliptic operator similar to the one occuring in our simple

Numerical Methods for Partial Differential Equations (Volume Number), 1–10 ((Year))

model equation. In these applications, due to nonlinear hyperbolic terms, control-volume formulations are prevailing.

The paper is organized as follows. In Section II, we discuss the discretization of the elliptic equation. The adaptive technique is discussed in Section III. Section IV contains numerical test runs and discussions on the convergence behavior. We also investigate the convergence of the conjugate gradient method for solution of the linear systems. A related discussion of the conjugate gradient method for refined grids can be found in [6].

II. DISCRETIZATION

We consider the boundary value problem

$$-\operatorname{div}(\mathbf{K}\operatorname{grad} p) = q \quad \text{in } \Omega, \tag{2.1}$$

$$p = p_0 \quad \text{on } \partial\Omega_{\mathrm{D}}, \tag{2.2}$$

$$-(\mathbf{K}\operatorname{grad} p)\cdot\mathbf{n} = u_0 \quad \text{on } \partial\Omega_{\mathrm{N}}, \tag{2.3}$$

where $\Omega \subset \mathbb{R}^2$ and $\partial\Omega_{\mathrm{D}} \cup \partial\Omega_{\mathrm{N}} = \partial\Omega$. Here, the conductivity $\mathbf{K}$ is a symmetric positive definite matrix with principal directions parallel to the x and y directions, i.e., in the coordinate system (x, y), the conductivity is the diagonal matrix $\mathbf{K} = \operatorname{diag}(k_x, k_y)$. In the applications, $\mathbf{K}$ will be piecewise constant. The vector $\mathbf{n}$ is the outer unit normal vector.

We equip the domain with a grid such that the union of the grid cells equals the domain. Integrating over the volume V_i of cell i, equation (2.1) reads

$$\sum_j f_{i,j} = \int_{V_i} q \, d\tau. \tag{2.4}$$

Here, $f_{i,j}$ is the flux across edge j of cell i, i.e.,

$$f_{i,j} = \int_{S_{i,j}} u \, d\sigma, \tag{2.5}$$

where $S_{i,j}$ is the surface of the edge and u is the flow density normal to the edge,

$$u = -(\mathbf{K}\operatorname{grad} p)\cdot\mathbf{n}. \tag{2.6}$$

We use the control-volume method to discretize equation (2.4). Initially, we apply a Cartesian grid, where the grid lines are aligned with the x and y directions. Figure 1 shows two cells whose common edge is normal to the x direction. For this edge, the conventional two-point flux approximation reads

$$f = T(p_1 - p_0), \tag{2.7}$$

where p_i is the potential at the center of cell i and T is the transmissibility between the two cells,

$$T = \frac{h_{1,y}}{\frac{1}{2}\left(\frac{h_{0,x}}{k_{0,x}} + \frac{h_{1,x}}{k_{1,x}}\right)}. \tag{2.8}$$

Here, $k_{i,x}$ is the conductivity of cell i in x direction. Further, $h_{i,x}$ and $h_{i,y}$ are the width of cell i in x and y direction, respectively. The formula (2.8) is derived by assuming

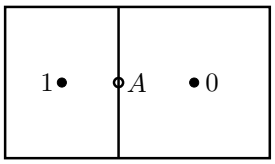

FIG. 1. Two cells.

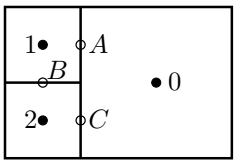

FIG. 2. Cell with two neighbors at one side.

linear potentials in the two cells 0 and 1, and requiring continuous flux and continuous potential at the point A of Figure 1.

To refine the grid in areas where the discretization error is large, cells may be divided into two or more equal subcells. We require that each cell may only have two refined cells at each side, as shown in Figure 2. The refined cells have the same conductivity values as the mother cell. To determine the flux across the edges between cell 1 and cell 0 and between cell 2 and cell 0 in Figure 2, we assume that the potentials in the three cells are linear and that flux and potential are continuous at the points A, B and C. The flux between cell 1 and cell 0 as well as the flux between cell 2 and cell 0 are then determined to

$$f = T\big(\tfrac{1}{2}(p_1 + p_2) - p_0\big), \tag{2.9}$$

where p_i is the potential at the center of cell i. The flux expression (2.8), (2.9) has earlier been applied in [9], but is there rendered with a misprint. We remark that we only derive the flux expression for the case of equal conductivities in cells 1 and 2. In case of different conductivities, a flux expression taking more cells into account, may be required [3].

Note that in case of a homogeneous medium, the flux approximations (2.7) and (2.9) are exact for linear pressure fields.

The two-point flux expression (2.7) yields a system of equations where the matrix of coefficients is a symmetric M-matrix. Refinement with the multipoint flux expression (2.9) leaves the matrix of coefficients symmetric, while the M-matrix property is retained for [9]

$$\sqrt{\frac{k_{1,x}}{k_{1,y}}}\,\frac{h_{1,y}}{h_{1,x}} \leq 1. \tag{2.10}$$

If the grid is constructed such that the left-hand side of inequality (2.10) is 1, refinement in both x and y direction can be performed, retaining the M-matrix property.

In the control-volume formulation (2.4), the treatment of the Neumann boundary condition (2.3) is straight forward. To treat the Dirichlet boundary condition (2.2), we introduce for each Dirichlet boundary cell a triangle with one corner at the cell center and the other two corners at the boundary corners of the cell, see Figure 3. Let the outer normal vectors of the edges of the triangle be denoted by $\mathbf{s}_k$, where the length of each normal vector is equal to the length of the edge to which it is normal. The vector $\mathbf{s}_k$ is normal to the edge opposite to corner k, $k = 1, 2, 3$, see Figure 3. The area of the triangle is denoted by A. The flux (2.5), (2.6) across the boundary edge may then be approximated by expressing the gradient in the boundary cell by

$$\operatorname{grad} p = -\frac{1}{2A}\sum_{k=1}^{3} p_k \mathbf{s}_k, \tag{2.11}$$

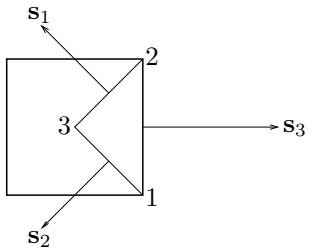

FIG. 3. Boundary cell with vectors $\mathbf{s}_k$.

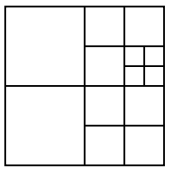

FIG. 4. Cell refinement.

where p_k is the potential value at corner k of the triangle.

III. ADAPTIVE TECHNIQUE

When discretizing the differential equation (2.1), it is advantageous to use a coarse grid in some areas and a finer grid in other areas. In an adaptive technique, the grid is refined according to some criterion, where the goal is to reduce the computational cost necessary to achieve a solution which satisfies some error bound. For each cell i, a refinement indicator ϵ_i is defined, and those cells with the largest values of ϵ_i are divided into smaller cells. The process is repeated until some stopping criterion is met.

When equation (2.1) is discretized with the finite element method, it is customary to use a residual-based refinement indicator [4, 5, 8, 18], see also [15]. For our control-volume method, this refinement indicator may be given as

$$\epsilon_i = \|q\|_{L^2(V_i)} |V_i|^{1/2} + \|u_h\|_{L^2(\partial V_i)} |\partial V_i|^{1/2} . \tag{3.1}$$

Here, u_h is the discrete approximation to (2.6), $|V_i|$ is the area of cell i and $|\partial V_i|$ is the length of the boundary of cell i. Note that u_h is already known through the discrete flux expressions (2.7) (2.9).

The first term in (3.1) measures the source term in a cell, and the second term in (3.1) measures the flux across the cell edges. However, unlike finite element methods, control-volume methods possess local conservation, and therefore, one may argue that the source term is contained in the flux term. A reasonable refinement indicator for control-volume methods is therefore given by the reduced expression

$$\epsilon_i = \|u_h\|_{L^2(\partial V_i)} |\partial V_i|^{1/2} . \tag{3.2}$$

In Section IV, we will compare the performance of the refinement algorithm, using the expressions (3.1) and (3.2).

To create a refinement algorithm, we define for each cell i an adaptivity index

$$\eta_i = \frac{\epsilon_i}{\max_j \epsilon_j}. \tag{3.3}$$

Obviously, $\eta_i \in [0, 1]$. At each iteration level, we refine all cells for which $\eta_i \geq \delta$, where δ is some prescribed tolerance between 0 and 1. In the test runs of Section IV, we have chosen $\delta = 0.6$.

When a cell is chosen for refinement, we devide the cell into two equal parts both vertically and horizontally, thus creating four equal subcells. Each of the four daugther

cells then has the same shape as the mother cell. Thus, if inequality (2.10) is satisfied for the initial grid, it will be satisfied for all grids in the refinement algorithm.

We require that each cell can have at most two neighboring cells at each side. To ensure that this criterion is fulfilled at each iteration level, additional cells may have to be refined. Figure 4 shows an example of a refined grid.

The behavior of the refinement algorithm can be measured by the error indicator

$$\xi_k = \max_i \epsilon_i, \qquad k = 0, 1, 2, \ldots, \tag{3.4}$$

where k is the iteration level. The ratio ξ_k/ξ_0 measures the reduction rate of the refinement indicator ϵ_i. Therefore, the condition $\xi_k/\xi_0 \leq \Delta$ may be used as a stopping criterion in the algorithm [8].

IV. NUMERICAL EXAMPLES

In this section, we test the adaptive algoritm described in Section III with the discretization of Section II. In all examples, we use an isotropic medium ($k_{i,x} = k_{i,y} = k_i$) and a grid with square grid cells ($h_{i,x} = h_{i,y} = h_i$). The initial grid is a 2×2 grid on a square domain.

The convergence of the algorithm is measured in L^2 and L^∞ norm for the potential and in L^2 norm for the flow density. The discrete L^2 norms are defined by

$$\|p_h - p\|_{L^2} = \left(\sum_i \|p_h - p\|^2_{L^2(V_i)} \right)^{1/2} \tag{4.1}$$

and

$$\|u_h - u\|_{L^2} = \frac{1}{2} \left(\sum_i \|u_h - u\|^2_{L^2(\partial V_i)} \, |\partial V_i| \right)^{1/2}, \tag{4.2}$$

where, as before, i is the cell index. Note that on uniform grids, the norm (4.2) equals 2 times the norm applied in [1] for the same quantity (disregarding boundary effects).

The number of degrees of freedom in the discrete system is denoted by DOF. At each iteration level, DOF equals the number of cells in the grid. We measure the convergence as a function of DOF, or rather as a function of $n = \mathrm{DOF}^{1/2}$. On a uniform square grid, n equals the number of grid cells in each coordinate direction.

In our first test case, we test the two refinement indicators (3.1) and (3.2) for a case where the source density, q, in equation (2.1) varies strongly. The medium is homogeneous with $k = 1$, and the domain is $[0, 1] \times [0, 1]$. We apply homogeneous Dirichlet boundary conditions. The source density q is chosen such that the exact solution becomes

$$p(x, y) = 0.0005[x(1 - x)y(1 - y)]^2 \, e^{10(x^2+y^2)}. \tag{4.3}$$

A similar solution has been studied in [15]. The convergence behavior of the flow density in the refinement algorithm is shown in Figure 5. The results for uniform grids is also shown. All test runs indicate a convergence rate

$$\|u_h - u\|_{L^2} \sim n^{-2}, \tag{4.4}$$

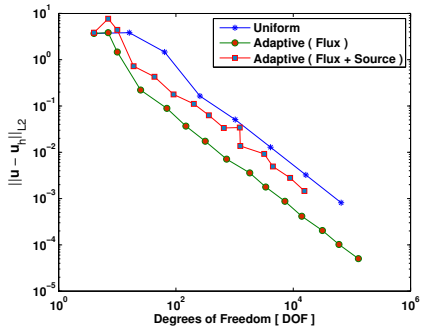

FIG. 5. Convergence behavior of example (4.3). L^2 error of the flow density.

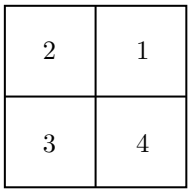

FIG. 6. Chessboard domain.

where $n = \mathrm{DOF}^{1/2}$, but the error using the adaptive methods is smaller than the error using uniform grids. Further, among the adaptive methods, the flux-based refinement indicator (3.2) produces the smallest error, as well as the fastest refinement. This indicates that of the two refinement indicators (3.1) and (3.2), the flux-based indicator (3.2) is to be preferred.

Our second test case has a strong heterogeneity, producing a solution with a low Sobolev regularity. For this case the source density, q, is zero. The domain $[-1,1]\times[-1,1]$ is divided into four equal squares as shown in Figure 6. The parts are enumerated as shown in the figure. The conductivity in part 1 and part 3 is k_1, and the conductivity in part 2 and part 4 is k_2. Thus, the domain is similar to the four squares of a chessboard. Let the distance from the origin be r and the angle from the x axis be θ. For $q = 0$ there exists a solution to (2.1) of the form

$$p(r,\theta) = cr^{\gamma} \begin{cases} \cos\gamma(\theta - \pi/4) & \text{for } \theta \in [0,\pi/2], \\ d\sin\gamma(3\pi/4 - \theta) & \text{for } \theta \in [\pi/2,\pi], \end{cases} \tag{4.5}$$

satisfying the symmetry relation $p(r,\theta) = -p(r,\theta-\pi)$. Here, c is an arbitrary constant, $\gamma = (4/\pi)\arctan(1/\sqrt{\kappa})$ and $d = \cos(\gamma\pi/4)/\sin(\gamma\pi/4)$, while $\kappa = k_1/k_2$ is the conductivity ratio. The solution belongs to the Sobolev space $H^{1+\alpha}$ for any $\alpha < \gamma$. The constant c has been chosen to $c = -\sin(\gamma\pi/4)$. This test case is a standard case for testing adaptive techniques with finite element methods [8, 13, 15]. We solve this problem for varying κ, using Dirichlet boundary conditions at the boundary parts 2 and 4 and Neumann boundary conditions at the boundary parts 1 and 3.

Figures 7, 8 and 9 show the convergence behavior on uniform grids for different values of γ in the solution (4.5). The test runs indicate the following asymptotic convergence rates for $\gamma \in (0,1]$,

$$\begin{aligned} \|p_h - p\|_{L^2} &\sim n^{-2\gamma}, \\ \|p_h - p\|_{L^\infty} &\sim n^{-\gamma}, \\ \|u_h - u\|_{L^2} &\sim n^{-\gamma}, \end{aligned} \tag{4.6}$$

where, as before, $n = \mathrm{DOF}^{1/2}$. The smaller γ is, the later the asymptotic region is entered. For $\gamma = 0.1$, the expected asymptotic behavior of the flow density error was

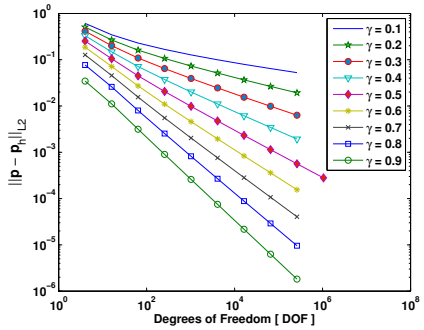

FIG. 7. Convergence of example (4.5) for uniform grids. L^2 error of the potential.

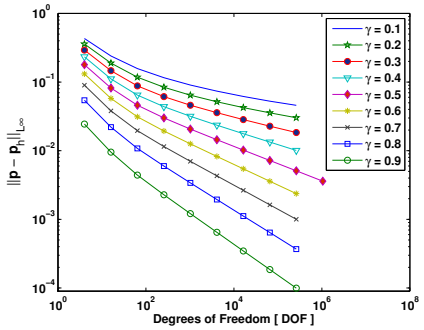

FIG. 8. Convergence of example (4.5) for uniform grids. L^∞ error of the potential.

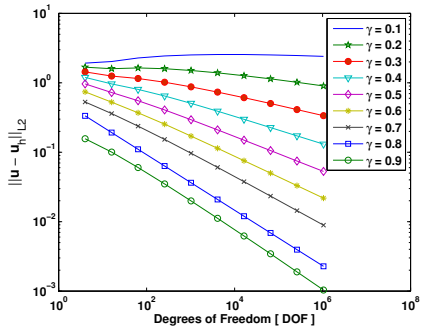

FIG. 9. Convergence of example (4.5) for uniform grids. L^2 error of the flow density.

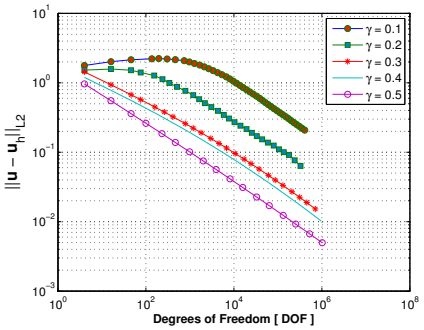

FIG. 10. Convergence of example (4.5) for adaptive grids. L^2 error of the flow density.

not reached for DOF $\leq 10^6$. The convergence behavior on uniform grids coincides with results reported in [1, 10] for the control-volume method. In [1], the rate $n^{-\gamma}$ for the errors $\|p_h - p\|_{L^\infty}$ and $\|u_h - u\|_{L^2}$ is reported to hold also for $p \in H^{1+\gamma}$, $\gamma \in [1, 2]$.

Figures 10, 11 and 12 show the convergence behavior for different values of γ in the solution (4.5), using the adaptive algorithm. The test runs indicate the following asymptotic convergence rates for $\gamma \in (0, 1]$,

$$\begin{aligned} \|p_h - p\|_{L^2} &\sim n^{-2}, \\ \|p_h - p\|_{L^\infty} &\sim n^{-1}, \\ \|u_h - u\|_{L^2} &\sim n^{-1}, \end{aligned} \tag{4.7}$$

where, as above, $n = \mathrm{DOF}^{1/2}$. The asymptotic region is entered earlier than for uniform grids. Equation (4.7) demonstrates achievable convergence rates for solutions in the Sobolev space $H^{1+\gamma}$, $\gamma \in (0, 1]$. A sequence of the adaptive grids for the case $\gamma = 0.1$ is shown in Figure 13.

Figure 14 shows the behavior of the error indicator (3.4) for different values of γ. For low refinement levels k, the indicator reduces rapidly. For higher values of k, large refinements in the grid are necessary to achieve a significant reduction in the error indicator.

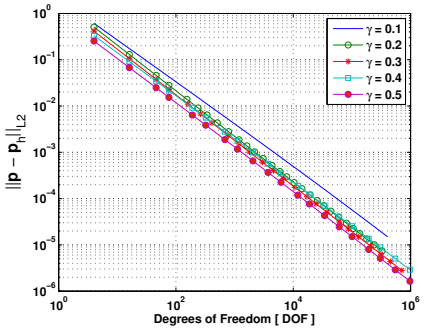

FIG. 11. Convergence of example (4.5) for adaptive grids. L^2 error of the potential.

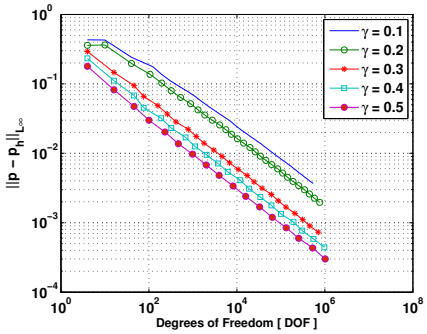

FIG. 12. Convergence of example (4.5) for adaptive grids. L^∞ error of the potential.

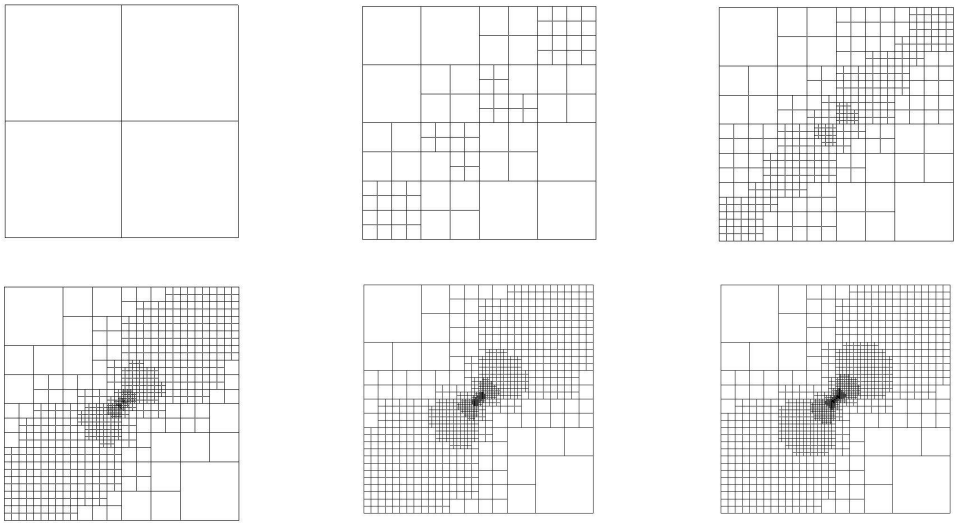

FIG. 13. Sequence of adaptive grids for the case $\gamma = 0.1$ for selected refinement levels.

The linear equations of the discrete formulation are solved with the conjugate gradient (CG) method. At each iteration level in the CG algorithm, the error in the norm defined by the matrix of coefficients is reduced by

$$\frac{1-\kappa^{-1/2}}{1+\kappa^{-1/2}} \approx 1 - 2\kappa^{-1/2}, \tag{4.8}$$

where κ is the spectral condition number of the matrix of coefficients. Hence, after m cycles of the CG iteration, the error is reduced by

$$r = \left(1 - 2\kappa^{-1/2}\right)^m \approx e^{-2m/\sqrt{\kappa}}. \tag{4.9}$$

It follows that

$$m \approx -\tfrac{1}{2}\sqrt{\kappa}\ln r. \tag{4.10}$$

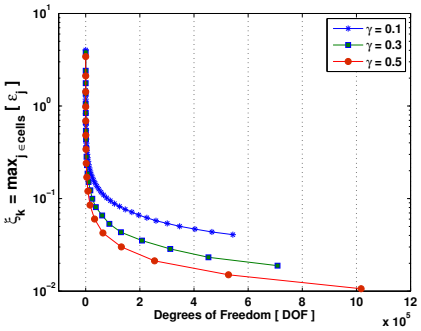

FIG. 14. Decrease in the error indicator (3.4) with adaptive refinement. k is the refinement level.

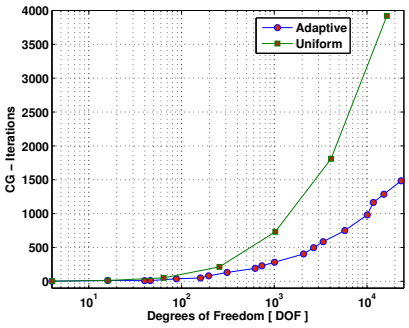

FIG. 15. Number of CG iteration cycles (without preconditioning) for uniform and adaptive grids. $\gamma = 0.1$.

In Figure 15, the number of CG iteration cycles is compared for uniform and adaptive grids for the case $\gamma = 0.1$. The diagram shows that for a given number of degrees of freedom, the number of iteration cycles required to solve the discrete system is approximately three times higher for the uniform grid than for the adaptive grid.

Denote the number of CG iteration cycles necessary to achieve a certain error bound by m_{u} for the uniform grid and by m_{a} for the adaptive grid. Similarly, let the spectral condition number of the matrix of coefficients be κ_{u} for the uniform grid and κ_{a} for the adaptive grid. From equation (4.10) it then follows that

$$\sqrt{\frac{\kappa_{\mathrm{u}}}{\kappa_{\mathrm{a}}}} \approx \frac{m_{\mathrm{u}}}{m_{\mathrm{a}}} \approx 3. \tag{4.11}$$

Hence, the ratio of the condition numbers is approximately nine. Thus, the applied adaptive algorithm does not only give better convergence rates than uniform grids. The discrete systems of the adaptive algorithm are also better conditioned.

V. CONCLUSIONS

In this work, numerical convergence of an adaptive algorithm for a control-volume method applied to elliptic equations has been studied. The test runs indicate that for solutions in the Sobolev space $H^{1+\gamma}$, $\gamma \in (0, 1]$, the convergence rate is second order for the potential in L^2 norm and first order for the potential in L^∞ norm and for the flow density in L^2 norm. Also, the system of linear equations is better conditioned for the adaptive grids than for uniform grids.

Finally, the refinement criterion in the algorithm has been discussed. The numerical tests indicate that a pure flux-based criterion is preferable.

REFERENCES

1. I. Aavatsmark, G. T. Eigestad, and R. A. Klausen. Numerical convergence of the MPFA O-method for general quadrilateral grids in two and three dimensions. In D. N. Arnold,

P. B. Bochev, R. Lehoucq, R. A. Nicolaides, and M. Shashkov, editors, *Compatible spatial discretizations*, IMA Vol. Ser., pages 1–21. Springer, New York, 2006.

2. I. Aavatsmark, G. T. Eigestad, R. A. Klausen, M. F. Wheeler, and I. Yotov. Convergence of a symmetric MPFA method on quadrilateral grids. 2005. Submitted to Comput. Geosci.
3. I. Aavatsmark, E. Reiso, and R. Teigland. Control-volume discretization method for quadrilateral grids with faults and local refinements. *Comput. Geosci.*, 5:1–23, 2001.
4. I. Babuška and A. Miller. A feedback finite element method with a posteriori error estimation. I. The finite element method and some basic properties of the a posteriori error estimator. *Comput. Methods Appl. Mech. Engrg.*, 61:1–40, 1987.
5. C. Bernardi and R. Verfürth. Adaptive finite element methods for elliptic equations with non-smooth coefficients. *Numer. Math.*, 85:597–608, 2000.
6. L. Bonaventura and G. Rosatti. A cascadic conjugate gradient algorithm for mass conservative, semi-implicit discretization of the shallow water equations on locally refined grids. *Int. J. Numer. Methods Fluids*, 40:217–230, 2002.
7. A. G. L. Borthwick, S. Cruz León, and J. Józsa. The shallow flow equations solved on adaptive quadtree grids. *Int. J. Numer. Methods Fluids*, 37:691–719, 2001.
8. Z. Chen and S. Dai. On the efficiency of adaptive finite element methods for elliptic problems with discontinuous coefficients. *SIAM J. Sci. Comput.*, 24:443–462, 2002.
9. M. G. Edwards. Elimination of adaptive grid interface errors in the discrete cell centered pressure equation. *J. Comput. Phys.*, 126:356–372, 1996.
10. G. T. Eigestad and R. A. Klausen. On the convergence of the multi-point flux approximation O-method: Numerical experiments for discontinuous permeability. *Numer. Methods Partial Diff. Eqns.*, 21:1079–1098, 2005.
11. R. E. Ewing, R. D. Lazarov, and P. S. Vassilevski. Local refinement techniques for elliptic problems on cell-centered grids. I. Error analysis. *Math. Comput.*, 56:437–461, 1991.
12. R. A. Klausen and R. Winther. Robust convergence of multi point flux approximations on rough grids. 2005. Submitted to Numer. Math.
13. P. Morin, R. H. Nochetto, and K. G. Siebert. Data oscillation and convergence of adaptive FEM. *SIAM J. Numer. Anal.*, 38:466–488, 2000.
14. D. W. Peaceman. *Fundamentals of Numerical Reservoir Simulation*. Elsevier, Amsterdam, 1977.
15. B. Rivière and M. F. Wheeler. A posteriori error estimates for a discontinuous Galerkin method applied to elliptic problems. *Comput. Math. Appl.*, 46:141–163, 2003.
16. G. Strang and G. J. Fix. *An Analysis of the Finite Element Method.* Prentice-Hall, Englewood Cliffs, NJ, 1973.
17. E. Süli. Convergence of finite volume schemes for Poisson's equation on nonuniform meshes. *SIAM J. Numer. Anal.*, 28:1419–1430, 1991.
18. R. Verfürth. *A Review of A Posteriori Error Estimation and Adaptive Mesh Refinement Techniques*. Wiley-Teubner, Stuttgart, 1996.
19. A. Weiser and M. F. Wheeler. On convergence of block-centered finite differences for elliptic problems. *SIAM J. Numer. Anal.*, 25:351–375, 1988.